Virtual Reality Backend for Operator Controlled Nanomanipulation

Bruno Sauvet*, Nizar Ouarti*, Sinan Haliyo and Stéphane Régnier
ISIR, Institut des Systèmes Intelligents et Robotique
Université Pierre et Marie Curie-Paris 6, CNRS-UMR 7222, Paris, France
Pyramide - T55/65, CC 173 - 4 Place Jussieu, 75005 Paris, France
Author e-mails: {sauvet, haliyo}@isir.upmc.fr
* These authors contributed equally to this work.

***Abstract*—Nanomanipulation is an important tool for recent developments in nanoscale production, characterization and analysis, both in material and life sciences. Its use is actually limited because of its complexity. Especially inside a scanning electron microscope, kinematic constraints, open-loop actuators and lack of natural visual access are barriers for its widespread use and require an operator specialized on a given set-up. The approach proposed here is to use a virtual model of such a manipulation set-up, synchronized in real-time with the real set-up, to overcome the difficulties for the operator to easily grasp and control his manipulation task. Moreover, such an approach would provide a virtual feedback to implement an overall closed loop control on the set-up.**

***Index Terms*—Nanomanipulation, open-loop control, virtual reality.**

I. Introduction

Actual nanotechnology fabrication relies mostly on deep-UV or electron-beam (e-beam) lithography. These process are proven successfully to produce a wide range of components and devices. Nevertheless, the lack of controlled assembly, fabrication intricacies and low throughput are posing persistent challenges to advance from a single device level to the functional circuit level. An additional issue in the nanoproduction process is the need to characterize physical, mechanical and electrical properties in the single component scale. Nanoscale manipulation is hence a key component for future advances in nanotechnology.

Nanoscale characterisation, especially in the R&D oriented processes is a non-repetitive and unautomated task. It is fundamentally user-driven and requires an operator to interact with the samples. This interaction spans several scales from nano to macroscopic level, involves generally a weakly automated kinematic chain for the manipulation and characterization tools and an indirect visual observation through high magnification optical or electron microscopes. Especially for the nanocharacterisation, manipulation stations inside scanning electron microcopes (SEM) has proven valuable tools [1]–[3]. Similar approaches has also emerged in biology, the ability provided by nanomanipulation to access the specimens at single molecule level hes led to interesting achievements [4]–[6].
Although it is similar to classical robotic remote handling, the additional constraints of scale reduction makes the overall operation a quite complicated task and difficult to perform.

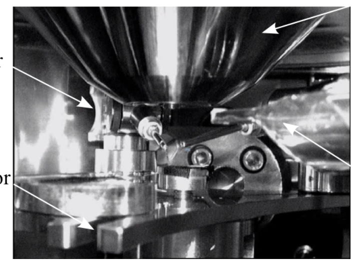

Figure 1. Inside a SEM chamber with a nanomanipulation set-up. The image is obtained by an integrated IR camera. It depicts the difficulty for an operator to grasp the 3D.

Fig. 1 shows typical a manipulation & characterisation station inside the specimen chamber of scanning electronic microscope (SEM) as illustration. This shown set-up uses fixed manipulators, and similar installations starts to appear in physics laboratories world-wide [7, 8]. Also some advanced set-ups, using for example mobile micro robots inside the SEM chamber [9] has been demonstrated. Other type of novel actuators specially designed for nanopositioning inside a SEM are also appearing in the literature [10].

The image is supplied by an integrated infrared camera and is typically what the operator is confronted with to perform the task. This video feed, in addition to the SEM image, is clearly not sufficient for a precision work. It is very difficult for the operator, if not impossible, to have a clear understanding of the tool motion that he's supposed to control, especially if several probes or tools in a complex 3D geometry are involved. In addition, in the exception of few especially designed specific set-ups, the kinematics are open-loop.

We propose here to tailor a specific virtual environment, in order to reproduce in 3D and real-time the specimen chamber, the sample holder and robotic tools of the manipulation set-up. The first advantage of such a virtual environment is to give the user an unlimited choice of his point of view enabling him to get a good grasp of his interaction. There are few examples in the literature on the use of virtual reality for nanomanipulation, which provides similar functionality [11]–[14]. This approach has also been used for remote nanomanipulation, between an operator in Paris, France and Oldenburg, Germany [15]. An additional advantage of a virtual environment as studied in the paper would be the possibility to implement an operator driven control scheme in order to overcome the limitations of open-loop nature of kinematics of the manipulator. As a further step, it would be possible to integrate virtual sensors in the environment, for example for a collision detection, distance measurement or evaluation of adhesion forces, in order to enhance the remote operation capabilities of such a nanomanipulation set-up.

In order to prove the concept of the intermediary virtual environment between a micro/nano-scale task and an operator, we describe here its implementation on a specific set-up, as show in Fig. 1. First, the architecture of such a manipulation system is discussed in the next section. Third section describes the details of the kinematics of the manipulation station and the proposed architecture for its virtual model. The real-time mapping between real and virtual set-ups are implemented using image processing techniques, described in the following section. An experimental validation of the proof of concept is presented afterwards.

II. Architecture

A micro/nano-manipulation set-up is complex system combining kinematic actuators, sensors, and visual observation. It covers several scales: the smallest is generally the component to be manipulated or characterized (thereafter referred as “the sample”); the manipulation and characterization tools (thereafter referred as “probes”) are generally an order of magnitude larger then the sample, carrying generally a sharp tip; actuators for probes and the sample holder are in a similar or often larger scale then probes; and finally the visual observation device, an optical or a scanning electron microscope.

All these components provide little to no feedback. Actuators are often open-loop devices who gives at best a single component position feedback difficult to interpret without a clear grasp of overall kinematics. Probes are basically sensors but geared towards the characterization of the sample, not their manoeuvrability. At best, in the case of AFM tips, they provide contact force information but limited to single axis. Microscopes are the main source of visual feedback but because of the very high magnification the image quality is low, with complete loss of depth information and a high noise-to-signal ratio in video feeds, especially in case of a SEM.

From a control point of view, considering the operator as the controller, a nanomanipulation set-up can be seen as a closed-loop system. However, this system has quite low performances because of the lack of quality of the feedback reaching the controller-operator. It also requires a certain skill and training on the operator for an acceptable efficiency.

We propose to insert a virtual model between the operator on the manipulators in order to improve the feedback and hence give to the operator a more intuitive and far easier way to interact. Two different architectures can be designed for this approach, as depicted in Fig. 2.

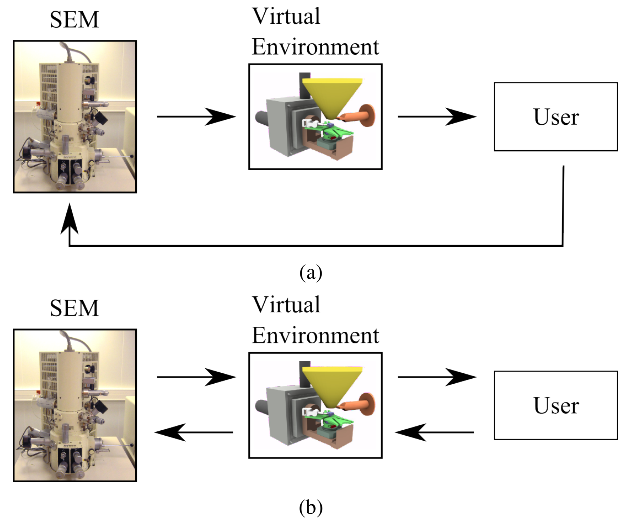

Figure 2. Architecture **A** : The user controls the manipulation stage. The configuration of virtual model is mapped on the real configuration. Architecture **B** : The user controls the virtual model. Its configuration is used as set-point for the real stage. This architecture uses a closed loop control between SEM and virtual environment and requires computer controlled actuators.

In the first architecture, the operator controls directly the kinematics of the manipulation station. Then, the kinematic configuration of virtual model is mapped automatically to the real configuration in real-time. The second architecture is a more advanced application case and requires to establish a closed loop control between the virtual model and the real set-up. In this case, the kinematic configuration of the virtual model is the set-point for the real set-up while virtual/real mapping is used to sole the control loop. The operator interacts solely with the virtual model while the real set-up is servoed to the virtual model.

The first architecture is obviously easier to implement and doesn’t require any specific automation on the real set-up. As long as one disposes of means to map the virtual model on the real set-up, event manual stages and actuators or open-loop manipulators can be used. On the other hand the second architecture implies a computer based control on the actuators. As the closed loop control would be implemented with real to virtual mapping, it is not required to dispose of closed-loop actuators, but manual stages which fits most SEMs are not usable.

In both architectures, the critical component is the mapping between the virtual model and the real set-up. In the first case, it would be implemented such as the virtual kinematic configuration would be controlled in order to minimize the mapping error and reproduce the kinematic configuration of the real set-up. In the second architecture, the virtual model is the reference configuration and the real stages and actuators are moved to minimize the mapping error.

In the following, we will focus on the issue of mapping between the virtual model and a real set-up. The proposed study is based on a worst-case scenario: the manipulation system, described in the next section, doesn't provide any position feedback, except video feeds from a SEM, and is fitted with a manual stage sample holder and open-loop Kleindiek manipulators. An image processing technique is proposed in order to map the motion of the sample holder to the virtual model.

III. Description of the manipulation set-up and its virtual model

This section gives the description of the manipulation set-up used for the proof-of-concept. The station is built inside the specimen chamber of SEM. The virtual model includes the chamber SEM's various components to reproduce faithfully the kinematic and volumetric constraints that the users are faced with during a manipulation task.

A. Manipulation station

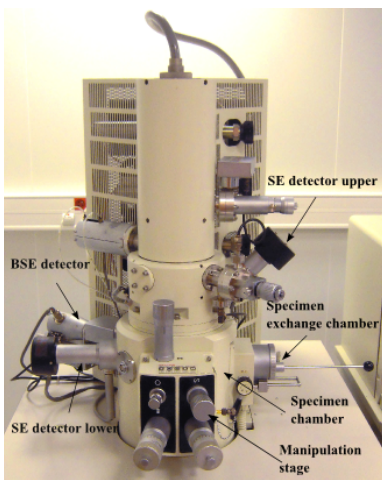

Figure 3. SEM Hitachi S4500 from outside. Several detectors for imaging are placed around the specimen chamber. The sample holder is manually operated with knobs in the center.

The SEM is a Hitachi S4500 (see Fig. 3). It is fitted with a cold-cathode field emission electron gun. A Everhart-Thornley secondary electrons detector is also used for sample observation. An InfraRed (IR) camera is located in specimen chamber to give a general view. Its acquisition frequency is 50 Hz; its resolution is 604*576 pixels; its focal length is 8.5 mm; and its wavelength is 88 nm.

The SEM is also fitted with a manual stage sample holder. The stage has 5 degres of freedom and are controlled by manual knobs as can be seen in Fig. 3:

- 3 translations:
  - X, Y axis (horizontal): travelling range $0 - 25$ mm; step 2 µm
  - Z axis (vertical): travelling range $3 - 28$ mm; step 20 µm
- 1 rotation on Z axis: travelling range $360°$; step $0.18°$
- 1 tilt on X axis: travelling range -$5 - 45°$; step $0.5°$

The manual stage supports the frame which can hold up to four micro-manipulators. The frame is made of 316L stainless steel to be vacuum compatible.

In the default configuration, used here, the frame is fitted with two Kleindiek (MM3A-EM) manipulators (Fig.4).

Each manipulator has 3 degrees of freedom and a travelling range of 5 nm on X axis, 3.5 nm on Y axis and 0.25 nm on Z axis. The actuation principle of Kleindeiks is piezo stick-slip principle. They are provided with an open-loop controller and they lack position feedback. A 30-pin vacuum feedthrough connects the manipulator to the external controller.

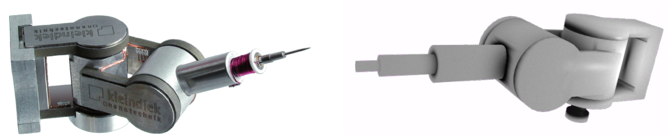

Figure 4. Kleindiek mm3a Micromanipulator and its 3D model

The frame is also fitted with an optical marker in order to assist the image processing (Fig.5). Its dimensions are $10 * 10$ mm. Its thickness is 1.96 mm. The pattern is formed by nine cubes, arranged by 3*3 in the center of the optical pattern. Cubes have dimensions of $1 * 1$ mm and each cube is separated by 1 mm.

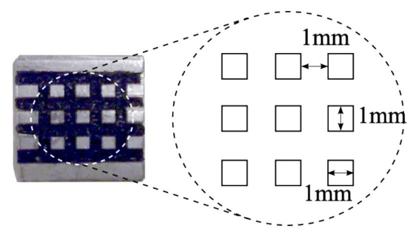

Figure 5. Marker designed for SEM. It is comprised of nine cubes. Their dimensions are $1 * 1$ mm, separated by 1 mm.

B. Virtual model

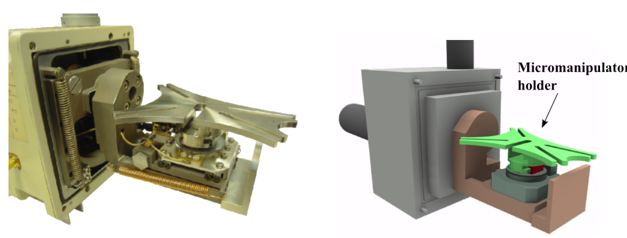

Figure 6. On the left, the real macromanipulation stage of SEM with macromanipulator holder. On the right, its virtual model.

Virtual model is constructed with *Blender*[1]. Blender includes an physics engine, with kinematics, collision

[1]Blender is a free open source software for 2D/3D modelisation. http://www.blender.org

detection and ray tracing based rendering. The model is designed with bindings allowing the external control of the kinematics of the sample holder and manipulators, reproducing faithfully the kinematics of the manipulation station. The physics-based render engine allows to mimic the optical and projection properties of a real camera and can produce virtual photographies, geometrically identical to their real counterparts.

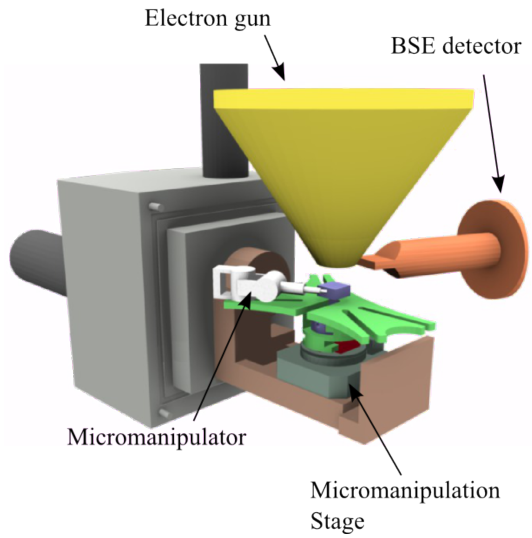

Figure 7. Full 3D modelisation of SEM chamber. Operator can move the view at will.

The model includes all the elements located in the specimen chamber of the SEM. In addition to micromanipulators (Fig. 4), the manipulation stage and the main frame (see Fig. 6), the canon beam and the BSE detector[2] are modeled as depicted in Fig. 7.
A collision detection algorithm is included in the virtual model with limits the motions of different elements and warns the user in case of proximity.

The model is fitted with a virtual camera, at the exact location of the IR camera of the specimen chamber, and with identical optical properties. This virtual camera hence gives virtual images of the model, with an identical projection of the real camera. the main advantage of this design is to be able to process comparatively real and virtual images.

IV. Image processing

In order to map the real set-up with its virtual model, an image processing technique is used. The aim is to find the 3D pose transform of a feature (in this case, the optical marker described above) between two images. As the virtual environment produces images with identical perspective and projection properties of the real set-up, this process can be conducted between two real images, two virtual virtual images or between a real and a virtual image.

[2]BSE detector : backscattered electron detector.

The principle is to extract interest points from the marker to define a disparity map between two views. The rotation and translation between these two views is then computed with an homography constraint and the *Posit* algorithm. A basic kinematic control loop on the virtual model can be used to minimize the disparity to map the real pose on the virtual model.

A. Feature extraction and Correspondences

Speeded Up Robust Features (SURF) is a technique that extracts robust features in an image [16]. The algorithm is based on the Haar wavelet [17]. Haar wavelet are 2D orthogonal wavelets with a vanishing moment of 1. The robust features are detected at different scales (scale-invariant) and the algorithm is also rotation-invariant. The principle is to approximate the determinant of Hessian blob detector [18]. The most important parameter of this algorithm is the threshold that conditions the number of accepted points. A too high threshold induces few points to be detected but these points have an high degree of robustness, similarly a too low threshold induce the detection of too many points. In the case of a SEM chamber, where lighting conditions are well controlled and stable, the points to detect are very robust. A relatively high threshold is a more appropriate choice.

The correspondences between detected points are then deduced with a sum of square difference (SSD) approach:

$$S = \sum_{\mathcal{I}} (I_1 - I_2)^2 \tag{1}$$

B. Computation of Homography Transformation

In order to compute the relative motion between two views, the homography transformation is calculated given the detected points. The homography constraint is applied on the given correspondences (x_1, x_2) such as:

$$\mathbf{x}_2 \times H\mathbf{x}_1 = 0 \tag{2}$$

With H the homography matrix, $\mathbf{x}_1$ $\mathbf{x}_2$ the homogeneous coordinates of the points pairs.

A threshold can be used to conserve the point pairs that are consistent with the homography (i.e. the points of the plane). It is important to obtain more than 3 points pairs, and to not obtain only collinear points in a given image.

The homography can be expressed with the following equation:

$$\mathbf{A}_i\mathbf{h} = 0 \tag{3}$$

With $\mathbf{h}$ vectorial form of the $\mathbf{H}$ matrix and:

$$A_i = \begin{bmatrix} 0^T & -w_i'\mathbf{x}_i^T & y_i'\mathbf{x}_i^T \\ w_i'\mathbf{x}_i^T & 0^T & -x_i'\mathbf{x}_i^T \\ -y_i'\mathbf{x}_i^T & x_i'\mathbf{x}_i^T & 0^T \end{bmatrix} \tag{4}$$

The coordinates of $\mathbf{x}'_i$ are x'_i, y'_i, w'_i, for a set of correspondences $\mathbf{x}_i$ and $\mathbf{x}'_i$.

To solve this equation, a Singular Value Decomposition (SVD) of A is used such as: $A = USV^T$. $\mathbf{h}$ will be the last column of V.

C. Determination of the Rotation and Translation

Based on the correspondence of the points of the plane, it is possible to deduce the rotation and the translation that occurred between the two images. *Posit* algorithm seems to be adequate for the computation of the orientation of the plane, as the real size and position of the points are known and the different points can be identified one from each other. The principle of *Posit* is to consider that the pose can be obtained from the equivalent of an orthographic projection, given a scale:

$$P_0P_i.I = x_i(1+\epsilon_i) - x_0 \tag{5}$$

$$P_0P_i.J = y_i(1+\epsilon_i) - y_0 \tag{6}$$

With P_0 the point of origin of the marker and P_i the other points of the marker.

$$I = \frac{f}{Z_0} i \tag{7}$$

$$J = \frac{f}{Z_0} j \tag{8}$$

$$\epsilon_i = \frac{1}{Z_0} P_0P_i.k \tag{9}$$

with $k = i \times j$.

The principle of the algorithm is that if ϵ is given, then the system composed by 6 can be solved where the only unknowns are I and J. Z_0 is found by the norm of I or J. To find ϵ the approximation of a scaled orthographic projection is done.

The iterative algorithm is as follows:

Algorithm 1 Pose Algorithm

while $|\epsilon_i(n) - \epsilon_i(n-1)| \geq threshold$ **do**
  Solve i, j, Z_0 with equation 6 and the constraint $i.j = 0$ (co-planar points)
  Compute $\epsilon_i = \frac{1}{Z_0} P_0P_i.k$ with $k = i \times j$
  $n = n + 1$
end while

The equations 6 can be rewritten in this form:

$$[U_iV_iW_i] \,.\, [I_uI_vI_w] = x_i(1+\epsilon_i) - x_0 \tag{10}$$

$$[U_iV_iW_i] \,.\, [J_uJ_vJ_w] = y_i(1+\epsilon_i) - y_0 \tag{11}$$

$U_iV_iW_i$ are the coordinates of the points P_i in the object coordinates frame of reference. $x_i, y_i, x_0 and y_0$ are the coordinates of the points p_i in the camera coordinates. These two equation can then be written as:

$$AI = x' \tag{12}$$

$$AJ = y' \tag{13}$$

$$I = A_{pi}x' \tag{14}$$

$$J = A_{pi}y' \tag{15}$$

With $A = [U_iV_iW_i]$ and $x' = x_i(1+\epsilon_i) - x_0$, $y' = y_i(1+\epsilon_i) - y_0$ Because the points are coplanar A have a rank of 2 and the set of equation is ill-determined. A constraint can be added which is: $i.j = 0$

A solution to this system that works for the coplanar case is:

$$I = I_0 + \lambda u \tag{16}$$

$$JI = J_0 + \mu u \tag{17}$$

With u is the null space of the matrix A.$[USV] = svd(A)$, u is the column vector of V that corresponds to the smallest singular value. I_0 and J_0 are the solution of equation 15.

Two unknown variables remains to be found: λ and μ, but there are two solutions for these variables [19]:

$$\lambda = \quad \rho cos\theta, \quad \mu = \quad \rho sin\theta \tag{18}$$

or

$$\lambda = \quad -\rho cos\theta, \quad \mu = \quad -\rho sin\theta \tag{19}$$

With :

$$\rho = ((J_0^2 - I_0^2)^2 + 4(J_0.I_0)^2)^{1/4} \tag{20}$$

Algorithm 2 ρ computation

$Re = J_0^2 - I_0^2$
$Im = -2J_0.I_0$
if $R > 0$ **then**
  $\rho = (arctan(Im/Re))/2$
end if
if $R < 0$ **then**
  $\rho = (arctan(Im/Re) + \pi)/2$
end if
if $R = 0$ **then**
  $\rho = sign(Im)\pi/2$
end if

V. Results

This method has been applied on a translation movement (see Fig.8, 9 and 10). The translation done by the stage is 0.5 mm ± 2 µm. A map is created by this method and a correspondence between images is determined (see Fig.11).

Many points will be removed from the disparity map. 1) The points that do not move between two frames. 2) The points that are not located in the binarised surface. 3) And the points that are not coherent with an homography.

Given the location of the points on the reference frame of the object, the Posit algortihm can now be applied. Another input for the algorithm is points (x_i, y_i) on the screen reference in pixels and the focal.

After computation, the distance determined for the translation between two positions of the marker is 0.4 mm. This result is close to the real movement (0.5 mm) given the observation distance (approximatively 10 cm) and the resolution and noise of the video. Also, the rotation matrix obtained is

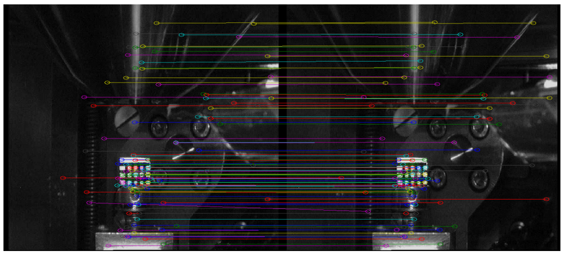

Figure 8. Correspondences between images. Static points were removed.

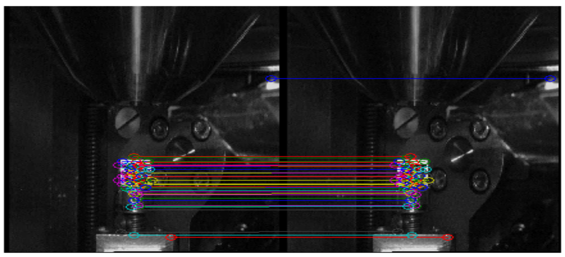

Figure 9. Correspondences between images. Points that belong to a region were the spatial gradient is important were preserved.

close to identity matrix, conforming to the lack of the rotation of the motion :

$$R = \begin{bmatrix} 0.9998 & -0.0070 & 0.0182 \\ 0.0126 & 0.9450 & -0.3268 \\ -0.0149 & 0.3270 & 0.9449 \end{bmatrix} \tag{21}$$

We found after reprojection of the points a mean error in pixels of 11.6 pixels. The reprojection consists of using the absolute coordinates in the object referential and to project the points

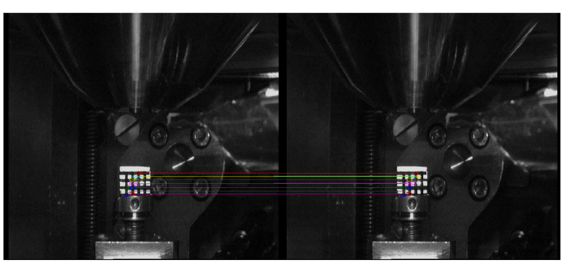

Figure 10. Correspondences between images. Points that are consistant with the homography constraint were preserved.

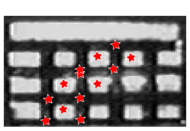

Figure 11. Each points in red are identified on a map. This allows to obtain the absolute location on the reference frame of the object in milimeters.

knowing the focal, the rotation matrix and the translation vector. The result is the coordinates in the screen referential. These coordinates can then be compared with the measured coordinates.

These results determined by computation still show a small margin of error in respect to the real displacement. To overcome this error, one solution is to reduce the noise in the data that was used for the computation. Actually, raw camera data is processed and a a noise filter would senibly improve the quality. Another improvement , given that the size of the object is very small compared to the distance from the camera, is to consider a strict orthographic projection.

VI. Conclusions and Future Work

Nanomanipulation is a valuable tool for research and development in material sciences and biology, especially inside a scanning electron microscope. However, the kinematic constraints, open-loop actuators and lack of natural visual access are barriers for its widespread use and require an operator specialized on a given set-up. We have proposed here an approach using an identical virtual model a real set-up in the aim to give the user a complete freedom of view of the manipulator. The virtual models mimics exactly the design of the manipulation set-up, including actuators with their kinematics, the manually operated sample-holder and diverse detectors inside the SEM chamber. Moreover, the virtual model includes also a reproduction of the infrared camera comprised in the SEM chamber, which produces images with identical projection.

In this paper, we have shown how to use those images, produced by both real and virtual cameras, to calculate a 3D kinematic transform between 2 two images. This process can be applied between two real or virtual images at t and $t+1$ frames, or between a real and a virtual images at the same frame in order to decrease the error between both images. This kinematic transform is then used to map the virtual model configuration to the real set-up's.

In this first demonstration of the proposed concept, only the manual stage is treated through image processing. Please note that the actuators of the current system are also open-loop and they do not provide position feedback. In the next iterations, it would be possible to combine the SEM image and the IR camera images to map the complete kinematics. In the case of use of actuators with complete or partial position feedback, the system can be further improved for very high fidelity.

VII. Acknowledgments

This work was supported by the French National Agency of Research, through the NANOROBUST project.

References

[1] F. Bussolotti, L. D'Ortenzi, V. Grossi, L. Lozzi, S. Santucci, and M. Passacantando, "In situ manipulation and electrical characterization of multiwalled carbon nanotubes by using nanomanipulators under scanning electron microscopy," *Phys. Rev. B*, vol. 76, no. 12, p. 125415, Sep. 2007.

[2] J.-C. Acosta, G. Hwang, J. Polesel-Maris, and S. Régnier, "A tuning fork based wide range mechanical characterization tool with nanorobotic manipulators inside a scanning electron microscope," *Review of Scientific Instruments*, vol. 82, no. 3, p. 035116 (8pp), 2011.

[3] X. Wei, Q. Chen, L. Peng, R. Cui, and Y. Li, "In situ measurements on individual thin carbon nanotubes using nanomanipulators inside a scanning electron microscope," *Ultramicroscopy*, vol. 110, no. 3, pp. 182 – 189, 2010.

[4] F. Iwata, Y. Mizuguchi, H. Ko, and T. Ushiki, "Nanomanipulation of biological samples using a compact atomic force microscope under scanning electron microscope observation," *Journal of Electron Microscopy*, vol. 60, no. 6, pp. 359–366, 2011.

[5] T. Fukuda and M. Nakajima, "Nanobioscience based on nanorobotic manipulation," in *Control Technologies for Emerging Micro and Nanoscale Systems*, ser. Lecture Notes in Control and Information Sciences, E. Eleftheriou and S. Moheimani, Eds. Springer Berlin / Heidelberg, 2011, vol. 413, pp. 169–180.

[6] T. Hirano, M. Nakajima, M. Kojima, N. Hisamoto, M. Homma, and T. Fukuda, "Selective nano-injection using nano-probe based on nanomanipulation under hybrid microscope," in *Micro-NanoMechatronics and Human Science (MHS), 2011 International Symposium on*, nov. 2011, pp. 216 –221.

[7] E. Meyer and H.-G. Braun, "Micro- and nanomanipulation inside the sem," *Journal of Physics: Conference Series*, vol. 126, no. 1, p. 012074, 2008. [Online]. Available: http://stacks.iop.org/1742-6596/126/i=1/a=012074

[8] H. Omori, M. Sadakata, I. Tsubokura, I. Hanasaki, and Y. Isono, "Development of in-situ sem nano manipulation amp; mems-based testing system with ultra-precision displacement sensors for nanomechanics of mwcnts," in *Micro Electro Mechanical Systems (MEMS), 2012 IEEE 25th International Conference on*, 29 2012-feb. 2 2012, pp. 412 –415.

[9] S. Fatikow, T. Wich, H. Hulsen, T. Sievers, and M. Jahnisch, "Microrobot system for automatic nanohandling inside a scanning electron microscope," *Mechatronics, IEEE/ASME Transactions on*, vol. 12, no. 3, pp. 244 –252, june 2007.

[10] V. Cherepanov, P. Coenen, and B. Voigtlander, "A nanopositioner for scanning probe microscopy: The koaladrive," *Review of Scientific Instruments*, vol. 83, no. 2, p. 023703, 2012. [Online]. Available: http://link.aip.org/link/?RSI/83/023703/1

[11] A. Ferreira, C. Cassier, and S. Hirai, "Automatic microassembly system assisted by vision servoing and virtual reality," *Mechatronics, IEEE/ASME Transactions on*, vol. 9, no. 2, pp. 321 –333, june 2004.

[12] M. Probst, C. Hürzeler, R. Borer, and B. J. Nelson, "Virtual reality for microassembly," in *Proceedings of SPIE, the International Society for Optical Engineering*. Society of Photo-Optical Instrumentation Engineers, 2007, pp. 67 180D.1–67 180D.10. [Online]. Available: http://cat.inist.fr/?aModele=afficheN&cpsidt=20634716

[13] M. Sitti, S. Horiguchi, and H. Hashimoto, "Nano tele-manipulation using virtual reality interface," in *Industrial Electronics, 1998. Proceedings. ISIE '98. IEEE International Symposium on*, vol. 1, jul 1998, pp. 171 –176 vol.1.

[14] A. Sulzmann and J. Jacot, "3D computer graphics based interface to real microscopic worlds for μ-robot telemanipulation and position control," in *Systems, Man and Cybernetics, 1995. Intelligent Systems for the 21st Century., IEEE International Conference on*, vol. 1, Oct. 1995, pp. 286 –291 vol.1.

[15] A. Bolopion, C. Stolle, R. Tunnell, S. Haliyo, S. Régnier, and S. Fatikow, "Remote microscale teleoperation through virtual reality and haptic feedback," in *2011 IEEE/RSJ International Conference on Intelligent Robots and Systems (IROS 2011)*, 2011, pp. 894 – 900.

[16] H. Bay, T. Tuytelaars, and L. Van Gool, "Surf: Speeded up robust features," in *Computer Vision - ECCV 2006*, ser. Lecture Notes in Computer Science, A. s. Leonardis, H. Bischof, and A. Pinz, Eds. Springer Berlin / Heidelberg, 2006, vol. 3951, pp. 404–417. [Online]. Available: http://www.springerlink.com/content/e580h2k58434p02k/abstract/

[17] T. Lindeberg, *Scale-Space Theory in Computer Vision*, 1994.

[18] I. Daubechies, *Ten Lectures on Wavelets (CBMS-NSF Regional Conference Series in Applied Mathematics)*. SIAM: Society for Industrial and Applied Mathematics, 1992.

[19] D. Oberkampf, D. DeMenthon, and L. Davis, "Iterative pose estimation using coplanar points," in *Computer Vision and Pattern Recognition, 1993. Proceedings CVPR '93., 1993 IEEE Computer Society Conference on*, 1993, pp. 626 –627.